An Analog Neural Network for Estimating Sea State or Wave Height from Inertial Sensor Data

Vassilis Alimisis, Andreas Papathanasiou, Georgios Georgousis and Paul P. Sotiriadis

Department of Electrical and Computer Engineering
National Technical University of Athens, Greece
E-mail: alimisisv@gmail.com, andr.papath77@gmail.com, geordag@otenet.gr, pps@ieee.org

***Abstract*—This research introduces an alternative approach to design low-power analog artificial neural networks with a power consumption of only 532nW. The proposed network consists of sigmoid activation function circuit, $\tanh$ approximation circuit along with a current comparator. In order to validate the behavior as an analog classifier, a real-time vessel dataset is used, achieving an accuracy of 86.50% in predicting true waves from inertial sensor data. Moreover, a comparative assessment among other analog classifiers is conducted, all trained on the same dataset. These models underwent training via a software-based implementation. The architecture was implemented using the TSMC 90nm CMOS process and simulated using the Cadence IC Suite.**

***Index Terms*—Inertial sensor data, analog VLSI design, sea state, wave height, power-efficiency, artificial neural network**

I. Introduction

Inertial sensors are crucial in aerospace, automotive, electronics, and wearables, measuring an object's acceleration, angular velocity, and orientation in an inertial frame [1]–[3]. They use accelerometers and gyroscopes for precise tracking, vital in navigation, motion analysis, and stabilization across fields like robotics, virtual reality, and healthcare due to their small size, low-power use, and high accuracy [4], [5].

With rising autonomy in maritime operations, inertial sensors are increasingly deployed [6]. They play a key role in estimating sea state or wave height by measuring vessel accelerations and angular velocities [7]. Analyzing a vessel's responses to waves yields essential data on wave height, frequency, and direction [8]. This real-time information aids vessel navigation in rough seas and benefits offshore operations like oil and gas exploration [7], [9]. The integration of inertial sensors in sea state estimation signifies the fusion of advanced sensor tech with maritime industry needs, highlighting innovation's impact in this critical sector [7], [9].

This study is driven by the need for energy-efficient [10] and compact inertial sensors crucial in estimating sea conditions or wave height [11], [12]. It introduces a alternative approach, more specifically a power-efficient ($532nW$) and low-voltage (0.6V) analog hardware artificial neural network (ANN) employing a sigmoid activation function. The architecture demonstrates promise, hitting an accuracy of 86.50%, ideal for battery-dependent sensor systems. Validated on real data from METIS Cyberspace Technology, this design is rigorously tested in a TSMC 90nm CMOS process using Cadence IC Suite for simulation. Its accuracy is verified against software-based methods and other analog classifiers, establishing its reliability and efficiency in real-world applications.

The structure of this paper unfolds as follows: Section II delves into the mathematical underpinnings pertinent to the analog integrated threshold classifier proposed in this work. Section III outlines the primary components and the envisaged architecture of the classifier. The validation of the proposed classifier is conducted in Section IV, leveraging a real-world sea state dataset derived from inertial sensors. This section also encompasses a comparative analysis between the hardware and software implementations, complemented by sensitivity tests. Section V offers a comparative study and engages in a comprehensive discussion. Finally, in Section VI, we draw concluding remarks that encapsulate the key findings and implications of this study.

II. Artificial Neural Network Model

An ANN, akin to the human brain's neural system, comprises interconnected layers of neurons [13]. Information flows from the input layer, traversing through hidden layers for intricate computations, culminating in the output layer for predictions or classifications. Through training via backpropagation, the network refines its parameters, minimizing errors between predicted and actual outcomes. ANNs excel in discerning complex patterns, finding applications in image recognition, speech processing, and predictive modeling, transforming various fields.

Mathematically, an ANN's core equations involve the weighted sum of inputs, addition of bias, and activation function to calculate a neuron's input in a feedforward network [13]. ANNs can be mathematically represented at different levels of abstraction. This can be represented as:

$$z_j = \sum_{i=1}^{n} w_{ij} x_i + b_j. \tag{1}$$

Where: z_j is the weighted sum for neuron j, w_{ij} represents the weight connecting neuron i to neuron j, x_i is the output of neuron i in the previous layer and b_j is the bias term for neuron j.

The output of a neuron in a feedforward network results from applying an activation function, such as the sigmoid function represented by:

$$a_j = \sigma(z_j) = \frac{1}{1 + e^{-z_j}}. \tag{2}$$

where: a_j is the neuron's output and σ signifies the $sigmoid$ function. In a feedforward network, each layer's outputs serve as inputs for the subsequent layer, calculated as:

$$x_j^{(l+1)} = \sigma(\sum_{i=1}^{n} w_{ij}^{(l)} x_i^{(l)} + b_j^{(l)}). \tag{3}$$

Here, $x_j^{(l)}$ represents the output of neuron j in layer l, $w_{ij}^{(l)}$ are the weights connecting neurons between layers l and $l+1$ and $b_j^{(l)}$ is the bias term for neuron j in layer l. These equations form the foundational computations within a feedforward ANN.

III. Proposed Architecture

In this section, the proposed analog implementation of the ANN is analysed. The introduced architecture is adaptable, capable of handling different quantities of input dimensions. The structure of the suggested classifier, depicted in Fig. 1, is tailored for a classification task with 2 classes and N_d input dimensions. The number of layers in each class is a hyper-parameter, typically determined through exploratory data analysis. For simplicity, it consists of 1 hidden layer in each class. The proposed architecture is composed of a (hidden layer) sigmoid activation function circuit (SAF) [14], [15] and tanh approximation (THL) [16], an output layer with a current comparator (CC) circuit [17], as depicted in Fig. 1. The threshold current ($I_{r,th}$) is used as a decision boundary between the two classes. The entire classifier is designed to operate with a supply voltage set at $V_{DD} = -V_{SS} = 0.3V$, and all transistors are biased in the sub-threshold region.

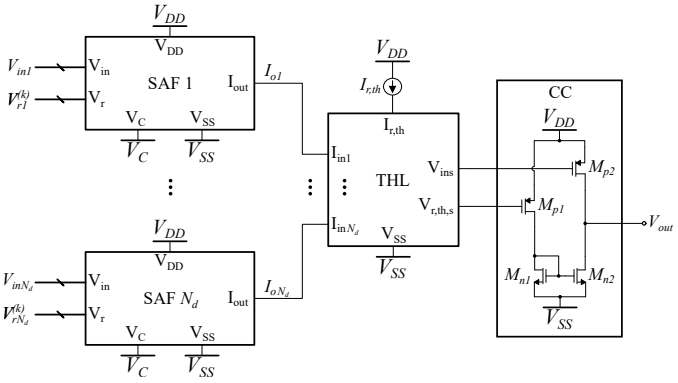

Fig. 1: The high level architecture of the proposed analog ANN.

Each sigmoid function circuit, illustrated in Fig. 2, serves the purpose of generating a univariate sigmoid function curve. This circuit comprises a PMOS cascode current mirror (consisting of transistors M_{p2},M_{p3} and M_{p5},M_{p6}), a NMOS cascode current mirror (consisting of transistors M_{n1} to M_{n4}) to ensure the production of high quality sigmoid curves, even for small bias currents and a simple differential pair M_{n7}, M_{n8} with two diode-connected triple-n-well transistors for variance tuning (V_c). Its electronic tuning capability provides precise control over the non-linear transformation function, offering both flexibility and accuracy in its behavior. The related simulation results are provided in Fig. 3. The I_{bias}, V_r and V_c parameters tunes the height, the mean value and the variance of the sigmoid function respectively. The dimensions of the transistors for a single sigmoid function circuit are summarized in Table I.

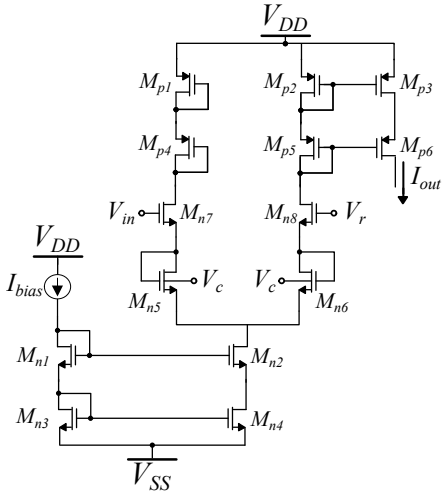

Fig. 2: The proposed sigmoid function circuit. It consists of two cascode current mirrors and an expanded differential pair.

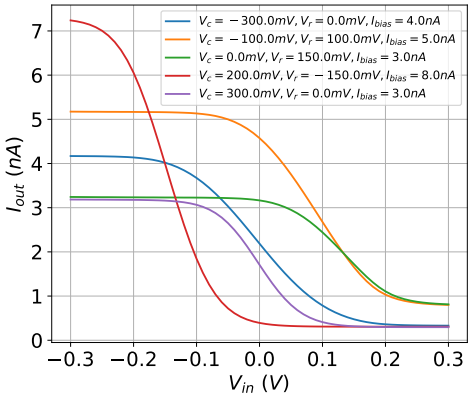

Fig. 3: The tunability in the output current via circuit parameters.

TABLE I: MOS Transistors' Dimensions (Fig. 2).

NMOS	W/L (µm/µm)	PMOS	W/L (µm/µm)
M_{n1}-M_{n6}	0.8/1.6	M_{p1}-M_{p6}	1.6/1.6
M_{n7}-M_{n8}	0.8/0.2	-	-

The second component in the hidden layer is a straightforward NMOS cascode current mirror with a PMOS diode load, which is shown in Fig. 4. Since all transistors operate in the sub-threshold region, this unit imparts an approximately tanh

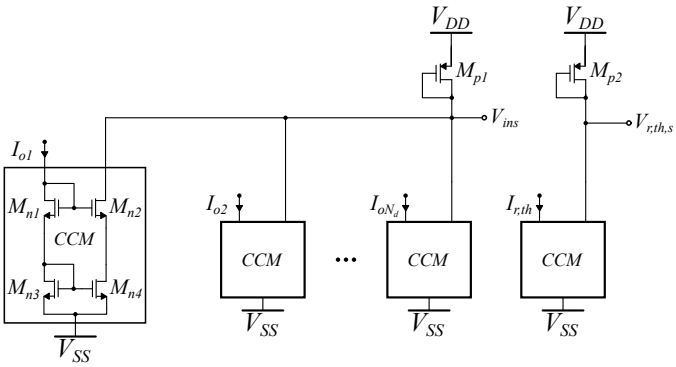

Fig. 4: The implementation of the $tanh$ approximation.

behavior to the output current of the SAF circuit. This method significantly trims down hardware expenses when compared to conventional circuit implementations of these activation functions. In the proposed ANN classifier, weight vectors are realized by adjusting the bias current I_{bias} of the preceding SAF circuit. For the first class, a set of N_d basic NMOS cascode current mirrors (CCMs) with a PMOS diode load is employed. This generates an output voltage called V_{ins}. For the decision boundary, a threshold current biases the CCM and provides an output voltage called $V_{r,th,s}$. The CC compares the two voltages, producing a final output voltage V_{out} (high or low depending on the winner).

IV. Sea State or Wave Height Application and Simulation Results

To assess the threshold classifier, a real-measurement dataset from METIS Cyberspace Technology was used, gathered from real-time naval vessel inertial readings. The dataset includes measurements for vessel hull heave displacement, speed, rolling angle and turn rate, surge displacement and speed, yaw turn rate, pitching angle, and pitch turn rate, each comprising 40320 instances. These measurements occur every 15 seconds per vessel hull instance. Derived from a combination of ML models [18] and parametric wave estimation [7], [9], the extracted features encompass peak-to-peak, crest factor, root mean square, shape factor, margin factor, skewness value, impulse factor, and kurtosis factor. For model training and testing, a $70-30\%$ split was implemented, resulting in 12096 test samples.

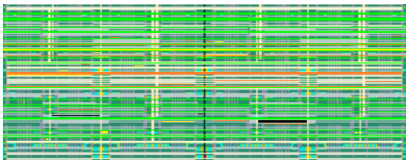

Fig. 5: The layout of the implemented classifier. Also, it consists of dummy transistors.

To evaluate the proposed classifier's performance amidst Process, Voltage, and Temperature (PVT) variations (both Monte Carlo and corners), two tests were conducted on the layout illustrated in Fig. 5. The layout's total area covers $0.041mm^2$. Results from 20 training-test iterations are depicted in Fig. 6 to encompass experimental variability. Regarding corners, it is tested under Typical, Slow, Fast cases (and combinations), for temperature variation of -25 to 125^oC and power-supply from $V_{DD} = -V_{SS} = 0.25V$ to $V_{DD} = -V_{SS} = 0.35V$. Moreover, a Monte Carlo analysis verifies the circuit's sensitivity, as shown in Fig. 7 with a Monte Carlo Histogram based on N = 100 data points. These tests collectively summarize the circuit's performance and resilience, presented in detail in Table II. Additionally, Fig. 8 displays snapshots showcasing wave height measurements and the classifier's predictions, including instances where the classifier made incorrect predictions (1 False prediction).

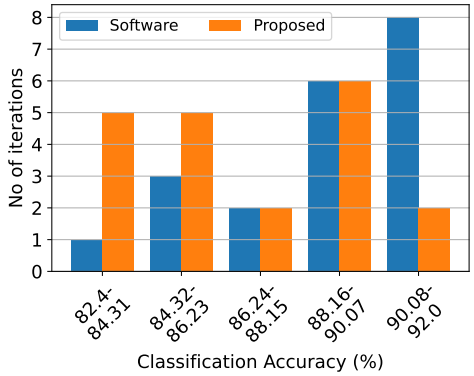

Fig. 6: Classification results of the proposed architecture and the equivalent software model on the dataset over 20 iterations.

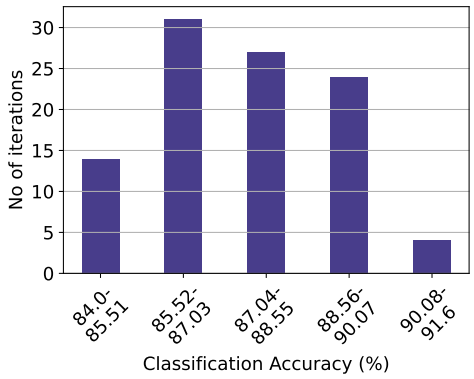

Fig. 7: Post-layout Monte-Carlo simulation results of the proposed architecture on the dataset.

TABLE II: Performance Results over PVT

Method	Best	Worst	Mean	Std.
Software	91.90%	83.80%	89.20%	1.03%
Proposed	90.70%	82.40%	86.50%	1.12%
Monte Carlo	91.60%	84.00%	87.35%	1.77%

V. Analog Classifiers Summary and Discussion

Analog classifiers often cater to specific applications, making unbiased comparisons challenging yet opening doors for

TABLE III: Analog classifiers' comparison on the Vessel dataset. It contains worst case corner results for the proposed classifier.

	Classifier	Worst accuracy	Mean accuracy	Best accuracy	Power consumption	Processing speed	Energy per classification	No. of Dimensions
This work	ANN	82.40%	86.50%	90.70%	$532nW$	$300K \frac{\text{classifications}}{\text{s}}$	$\frac{1.77 \text{ pJ}}{\text{classification}}$	8
[19]	MLP	84.60%	87.32%	91.30%	$215.14\mu W$	$930K \frac{\text{classifications}}{\text{s}}$	$\frac{231.33 \text{ pJ}}{\text{classification}}$	8
[20]	ANN	73.30%	77.42%	80.30%	$1.43\mu W$	$3M \frac{\text{classifications}}{\text{s}}$	$\frac{0.48 \text{ pJ}}{\text{classification}}$	8
[21]	LSTM	92.10%	96.13%	100.00%	$15.18mW$	$870M \frac{\text{classifications}}{\text{s}}$	$\frac{17.45 \text{ pJ}}{\text{classification}}$	8
[22]	RBF	76.70%	80.43%	82.60%	$17.95\mu W$	$200K \frac{\text{classifications}}{\text{s}}$	$\frac{89.75 \text{ pJ}}{\text{classification}}$	8
[23]	K-means	81.80%	87.33%	91.20%	$67.78\mu W$	$5M \frac{\text{classifications}}{\text{s}}$	$\frac{13.56 \text{ pJ}}{\text{classification}}$	8
[24]	Bayes	73.80%	78.67%	81.40%	$573nW$	$100K \frac{\text{classifications}}{\text{s}}$	$\frac{5.73 \text{ pJ}}{\text{classification}}$	8
[25]	Fuzzy	78.40%	82.34%	87.90%	$689nW$	$4.55K \frac{\text{classifications}}{\text{s}}$	$\frac{151.43 \text{ pJ}}{\text{classification}}$	8
[26]	Centroid	81.30%	82.45%	86.40%	$683nW$	$100K \frac{\text{classifications}}{\text{s}}$	$\frac{6.83 \text{ pJ}}{\text{classification}}$	8
[27]	GMM	77.20%	80.83%	83.60%	$612nW$	$100K \frac{\text{classifications}}{\text{s}}$	$\frac{6.12 \text{ pJ}}{\text{classification}}$	8
[28]	Threshold	78.20%	79.47%	83.90%	$312nW$	$100K \frac{\text{classifications}}{\text{s}}$	$\frac{3.12 \text{ pJ}}{\text{classification}}$	8
[29]	SVM	79.60%	80.65%	81.60%	$45.42\mu W$	$140K \frac{\text{classifications}}{\text{s}}$	$\frac{324.43 \text{ pJ}}{\text{classification}}$	8

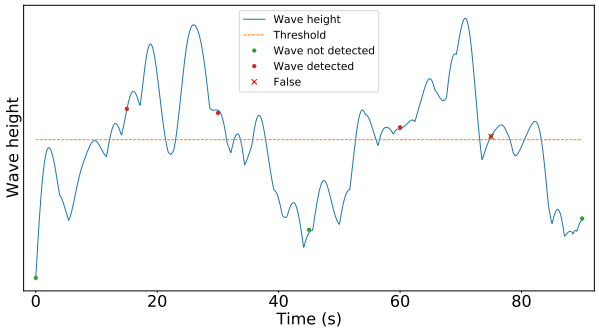

Fig. 8: Here, a specific number of snapshots related to the state of the sea are presented. They consist of wave height based on the measurements and indicate whether the measurement represents a wave or not. The inertial sensors provide a measurement every 15 seconds, and this measurement is classified (as a wave or not) by the proposed classifier. The classifier makes an incorrect prediction (False) for one of the measurements.

adaptable use in shared contexts. Notably, Table III offers a comprehensive overview of our study's performance metrics alongside comparable classifiers like Multilayer Perceptron (MLP) [19], ANN [20], Long Short-Term Memory (LSTM) [21], Radial Basis function [22], K-means [23], Bayesian [24], Fuzzy [25], Centroid-based [26] Gaussian Mixture Model (GMM) [27], Gaussian Threshold [28] and Support Vector Machine (SVM) [29] all within the context of sea state or wave height application dataset. This work, detailed in Table III, demonstrates a balanced performance in accuracy, power efficiency, and energy consumption.

This work, while excelling in accuracy comparable to several counterparts like MLP [19], LSTM [21], and K-means [23], achieves this with lower complexity, power usage, and chip area due to its simpler design. This simplicity allows for binary classification without dimensionality reduction, unlike many other models. Although some models attain higher accuracy, they do so at the cost of increased complexity, power consumption, and larger silicon area. The proposed classifier emphasizes lower power consumption and optimized energy use per classification, prioritizing accuracy over rapid processing speed, aligning well with the sporadic nature of inertial sensor applications. Notably, the Gaussian Threshold [28] achieves the lowest power consumption, but it achieves lower performance.

VI. Conclusion

In this study, an analog integrated neural network was introduced, characterized by its ultra-low power consumption at only 532nW and its reliance on SAF. The core components of this classifier comprise circuits implementing the sigmoid function, a $tanh$ approximation and current comparison. To validate its performance, a real-time vessel dataset capturing measurements in real-world scenarios is utilized. The post-layout simulations were performed using the TSMC 90nm CMOS process, enabling a thorough comparison with software-based implementations and a wide range of analog classifiers. Remarkably, the proposed implementation achieved a high accuracy rate of 86.50%, highlighting its potential as a crucial element within inertial sensor systems.

VII. Acknowledgements

This research has been co-financed by the European Union - NextGenerationEU and Greek national funds through the Greece 2.0 National Recovery and Resilience Plan, under the call RESEARCH-CREATE-INNOVATE (PROJECT CODE: TAEDK-06165). The authors would like to acknowledge METIS Cyberspace Technology Corporation for providing the data from real-time vessel measurements.

REFERENCES

[1] N. El-Sheimy and A. Youssef, "Inertial sensors technologies for navigation applications: State of the art and future trends," *Satellite Navigation*, vol. 1, no. 1, pp. 1–21, 2020.

[2] J. Collin, P. Davidson, M. Kirkko-Jaakkola, and H. Leppäkoski, "Inertial sensors and their applications," *Handbook of Signal Processing Systems*, pp. 51–85, 2019.

[3] M. Kok, J. D. Hol, and T. B. Schön, "Using inertial sensors for position and orientation estimation," *arXiv preprint arXiv:1704.06053*, 2017.

[4] M. Iosa, P. Picerno, S. Paolucci, and G. Morone, "Wearable inertial sensors for human movement analysis," *Expert review of medical devices*, vol. 13, no. 7, pp. 641–659, 2016.

[5] K. Papafotis, D. Nikitas, and P. P. Sotiriadis, "Improving gyroscope's noise performance using multiple accelerometers in a closed-loop configuration," *IEEE Sensors Journal*, vol. 22, no. 22, pp. 22 062–22 068, 2022.

[6] R. W. Button, J. Kamp, T. B. Curtin, and J. Dryden, "A survey of missions for unmanned undersea vehicles," *National Defense Research Institute. RAND Corporation*, vol. 223, 2009.

[7] L. Zago, A. N. Simos, A. Kawano, and A. M. Kogishi, "A new vessel motion based method for parametric estimation of the waves encountered by the ship in a seaway," *Applied Ocean Research*, vol. 134, p. 103499, 2023.

[8] H.-M. Heyn, M. Blanke, and R. Skjetne, "Ice condition assessment using onboard accelerometers and statistical change detection," *IEEE Journal of Oceanic Engineering*, vol. 45, no. 3, pp. 898–914, 2019.

[9] U. D. Nielsen and J. Dietz, "Ocean wave spectrum estimation using measured vessel motions from an in-service container ship," *Marine Structures*, vol. 69, p. 102682, 2020.

[10] M. Noreikis, Y. Xiao, and A. Ylä-Jääski, "Seenav: Seamless and energy-efficient indoor navigation using augmented reality," in *Proceedings of the on Thematic Workshops of ACM Multimedia 2017*, 2017, pp. 186–193.

[11] M. Marin-Perianu, S. Chatterjea, R. Marin-Perianu, S. Bosch, S. Dulman, S. Kininmonth, and P. Havinga, "Wave monitoring with wireless sensor networks," in *2008 International Conference on Intelligent Sensors, Sensor Networks and Information Processing*. IEEE, 2008, pp. 611–616.

[12] J. P. Mishra, K. Singh, and H. Chaudhary, "Research advancements in ocean environmental monitoring systems using wireless sensor networks: a review," *TELKOMNIKA (Telecommunication Computing Electronics and Control)*, vol. 21, no. 3, pp. 513–527, 2023.

[13] C. M. Bishop and N. M. Nasrabadi, *Pattern recognition and machine learning*. Springer, 2006, vol. 4, no. 4.

[14] B. Gilbert, "Translinear circuits: An historical overview," *Analog Integrated Circuits and Signal Processing*, vol. 9, pp. 95–118, 1996.

[15] E. Seevinck and R. J. Wiegerink, "Generalized translinear circuit principle," *IEEE journal of solid-state circuits*, vol. 26, no. 8, pp. 1098–1102, 1991.

[16] A. G. Andreou and K. A. Boahen, "Translinear circuits in subthreshold mos," *Analog Integrated Circuits and Signal Processing*, vol. 9, pp. 141–166, 1996.

[17] F. Yu, L. Gao, L. Liu, S. Qian, S. Cai, and Y. Song, "A 1 v, 0.53 ns, 59 μw current comparator using standard 0.18 μm cmos technology," *Wireless Personal Communications*, vol. 111, no. 2, pp. 843–851, 2020.

[18] B. Panić, J. Klemenc, and M. Nagode, "Gaussian mixture model based classification revisited: Application to the bearing fault classification." *Journal of Mechanical Engineering/Strojniški Vestnik*, vol. 66, no. 4, 2020.

[19] K. Lee, J. Park, and H.-J. Yoo, "A low-power, mixed-mode neural network classifier for robust scene classification," *Journal of Semiconductor Technology and Science*, vol. 19, no. 1, pp. 129–136, 2019.

[20] S. T. Chandrasekaran, R. Hua, I. Banerjee, and A. Sanyal, "A fully-integrated analog machine learning classifier for breast cancer classification," *Electronics*, vol. 9, no. 3, p. 515, 2020.

[21] Z. Zhao, A. Srivastava, L. Peng, and Q. Chen, "Long short-term memory network design for analog computing," *ACM Journal on Emerging Technologies in Computing Systems (JETC)*, vol. 15, no. 1, pp. 1–27, 2019.

[22] S.-Y. Peng, P. E. Hasler, and D. V. Anderson, "An analog programmable multidimensional radial basis function based classifier," *IEEE Transactions on Circuits and Systems I: Regular Papers*, vol. 54, no. 10, pp. 2148–2158, 2007.

[23] R. Zhang and T. Shibata, "An analog on-line-learning k-means processor employing fully parallel self-converging circuitry," *Analog Integrated Circuits and Signal Processing*, vol. 75, pp. 267–277, 2013.

[24] V. Alimisis, G. Gennis, C. Dimas, and P. P. Sotiriadis, "An analog bayesian classifier implementation, for thyroid disease detection, based on a low-power, current-mode gaussian function circuit," in *2021 International conference on microelectronics (ICM)*. IEEE, 2021, pp. 153–156.

[25] E. Georgakilas, V. Alimisis, G. Gennis, C. Aletraris, C. Dimas, and P. P. Sotiriadis, "An ultra-low power fully-programmable analog general purpose type-2 fuzzy inference system," *AEU-International Journal of Electronics and Communications*, vol. 170, p. 154824, 2023.

[26] V. Alimisis, V. Mouzakis, G. Gennis, E. Tsouvalas, C. Dimas, and P. P. Sotiriadis, "A hand gesture recognition circuit utilizing an analog voting classifier," *Electronics*, vol. 11, no. 23, p. 3915, 2022.

[27] V. Alimisis, G. Gennis, K. Touloupas, C. Dimas, M. Gourdouparis, and P. P. Sotiriadis, "Gaussian mixture model classifier analog integrated low-power implementation with applications in fault management detection," *Microelectronics Journal*, vol. 126, p. 105510, 2022.

[28] V. Alimisis, G. Gennis, E. Tsouvalas, C. Dimas, and P. P. Sotiriadis, "An analog, low-power threshold classifier tested on a bank note authentication dataset," in *2022 International Conference on Microelectronics (ICM)*. IEEE, 2022, pp. 66–69.

[29] V. Alimisis, G. Gennis, M. Gourdouparis, C. Dimas, and P. P. Sotiriadis, "A low-power analog integrated implementation of the support vector machine algorithm with on-chip learning tested on a bearing fault application," *Sensors*, vol. 23, no. 8, p. 3978, 2023.